A Computational Efficient General Wheel-Rail Contact Detection Method

João Pombo
IDMEC Instituto Superior Técnico, Av. Rovisco Pais 1, 1049-001 Lisboa, Portugal
Jorge Ambrósio*
IDMEC Instituto Superior Técnico, Av. Rovisco Pais 1, 1049-001 Lisboa, Portugal

The development and implementation of an appropriate methodology for the accurate geometric description of track models is proposed in the framework of multibody dynamics and it includes the representation of the track spatial geometry and its irregularities. The wheel and rail surfaces are parameterized to represent any wheel and rail profiles obtained from direct measurements or design requirements. A fully generic methodology to determine, online during the dynamic simulation, the coordinates of the contact points, even when the most general three dimensional motion of the wheelset with respect to the rails is proposed. This methodology is applied to study specific issues in railway dynamics such as the flange contact problem and lead and lag contact configurations. A formulation for the description of the normal contact forces, which result from the wheel-rail interaction, is also presented. The tangential creep forces and moments that develop in the wheel-rail contact area are evaluated using : Kalker linear theory ; Heuristic force method ; Polach formulation. The methodology is implemented in a general multibody code. The discussion is supported through the application of the methodology to the railway vehicle ML95, used by the Lisbon metro company.

Key Words : Railway Dynamics, Multibody Dynamics, Contact Mechanics, Rail-Wheel Contact

1. Introduction

In railway vehicle dynamics, the wheel-rail interaction plays a crucial role since the railway vehicle is guided by the forces generated by such contact. The problems to consider when studying the wheel-rail contact are :

(a) The contact geometry, i.e., the problem of determining the location of the contact point on the profiled surfaces using geometric contact constraints.

(b) The contact kinematics, i.e., the problem of defining the creepages at the point of contact.

(c) The contact mechanics, i.e., the problem of determining the tangential creep forces and the spin creep moment.

Several authors (Kalker, 1990 ; Polach, 1999 ; Kik, 1996) studied the contact forces between the wheel and the rail making available several computer routines for the calculations of the tangential forces at the contact point given the normal force and the relative velocities between the contacting bodies (Kalker, 1990 ; Polach, 1999). The problem here is reduced to provide descriptions of the surfaces in contact and of the kinematics of the bodies.

* Corresponding Author,
E-mail : jpombo@dem.ist.utl.pt
TEL : +351-21-8417680; **FAX** : +351-21-8417915
IDMEC Instituto Superior Técnico, Av. Rovisco Pais 1, 1049-001 Lisboa, Portugal. (Manuscript **Received** November 29, 2004; **Revised** December 15, 2004)

The track centerline geometry may be described by different types of parametric curves such as cubic, Akima or shape preserving splines. The track description adopted uses Frenet frames that provide the appropriate referential at every point and the definition of the cant angle variation along the railway. A pre-processor is used to define the nominal geometry of both left and right rails based on the interpolation of a discrete number of points, which are representative of their space curves (Pombo, 2003a, b). For the complete representation of the track geometry, both rails are considered separate geometric entities. For efficiency, a pre-processor generates a table with all track position data and other quantities required for the multibody code as function of the left and right rail lengths. During a dynamic simulation the program interpolates linearly both rails databases to obtain the information necessary to find the wheel/rail interaction. The coordinates of the contact points are evaluated during the dynamic analysis by introducing surface parameters that describe the geometry of the rail and wheel contact surfaces, each described by two surface parameters (Pombo, 2003b). The methodology allows the existence of two or more points of simultaneous contact between the wheel and the rail in the wheel tread or flange.

The normal contact forces that develop in the wheel-rail interface are calculated using the Hertz contact force model with hysteresis damping to account for the dissipation of energy during contact (Lankarani, 1994). The creepages, or normalized relative velocities at the contact point, are used with the normal contact force to determine the creep forces and the spin creep moment. Three different methodologies are implemented in order to calculate these tangential contact forces. These are the Kalker linear theory (Kalker, 1979 ; 1990), the Heuristic nonlinear creep force model (Shen, 1983) and the Polach formulation (Polach, 1999).

The methodologies proposed here are implemented in a general multibody code that is used for the dynamic analysis of rail-guided vehicles. Finally, the computer code is applied to the study of a railway vehicle in what its dynamics and stability is concerned.

2. Parameterization of Railway Track

A pre-processor program defines the track model as two parameterized curves that represent the nominal geometry of the left and right rails space curves. Parametric track descriptions using different types of splines are available (Pombo, 2003c). The information is organized in two databases where all quantities, necessary to define the rails curves, are function of the arc length of each rail, measured from their origin. The methodology is summarized as :

(a) The geometry of the track centerline is parameterized using a piecewise cubic interpolation scheme.

(b) The track cant angle is parameterized as function of the track length.

(c) The track centerline is also parameterized as function of the track length (Pombo, 2003c).

(d) The track irregularities, measured experimentally, are parameterized as continuum functions of the track length

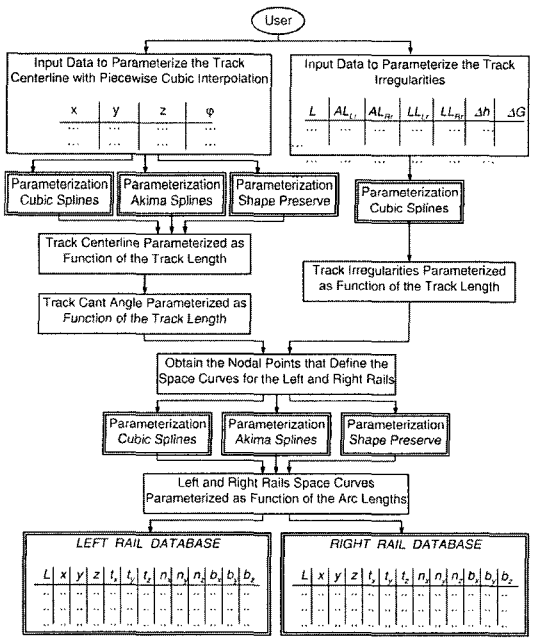

Fig. 1 Flowchart of the railway pre-processor

(e) Define a set of control points that are representative of the left and right rails space curves.

(f) Parameterize the rails space curves as a function of the arc lengths. Account for the track cant angle and rail inclination.

(g) Create a database for each rail, stored with a small track length step.

A schematic representation of the methodology used in the railway pre-processor is presented in Figure 1. The interested reader is referred to the work of Pombo and Ambrosio (2003a,b).

3. Wheel and Rail Surfaces

The definition of the wheel and rail needs to satisfy three main requirements. First, the surfaces have to be defined in a global coordinate system. Second, the parametric equations must be able to represent any spatial configuration of the wheelsets and rails. Third, the representation of any wheel and rail profiles, obtained by measurements or design requirements, must be possible.

Let two sets of independent surface parameters be used to define the geometry of each of the wheel and rail in contact be S_r and u_r, for the rail surface geometry, and S_w and u_w, for the wheel surface, as shown in Figure 2. The position vector of a contact point Q, in the wheel or rail body fixed coordinates systems, is function of the surface parameters only

$$\mathbf{u}_l = \mathbf{u}_l(s_l, u_l);\ l = r,\ w \tag{1}$$

where the subscripts $(.)_r$ and $(.)_w$ are referred to the rail and to the wheel respectively whereas the subscript $(.)_{ws}$ are referred to the wheelset.

In order to account for any possible scenarios, such as a variation in the gauge or relative displacements and/or rotations of the rails due to the track irregularities, it is necessary to define the surface of each rail independently, as depicted by Figure 3, where subscripts $(.)_{Lr}$ and $(.)_{Rr}$ are referred to the left and right rails respectively.

Let a profile coordinate system be defined on each rail to identify the position and orientation of any cross section along the rail space curve and P be a point of contact with the wheel. The right profile coordinate system $(\xi_{Rr}, \eta_{Rr}, \zeta_{Rr})$, shown in Figure 3, translates along a rail space curve and rotates about its origin. The location of the

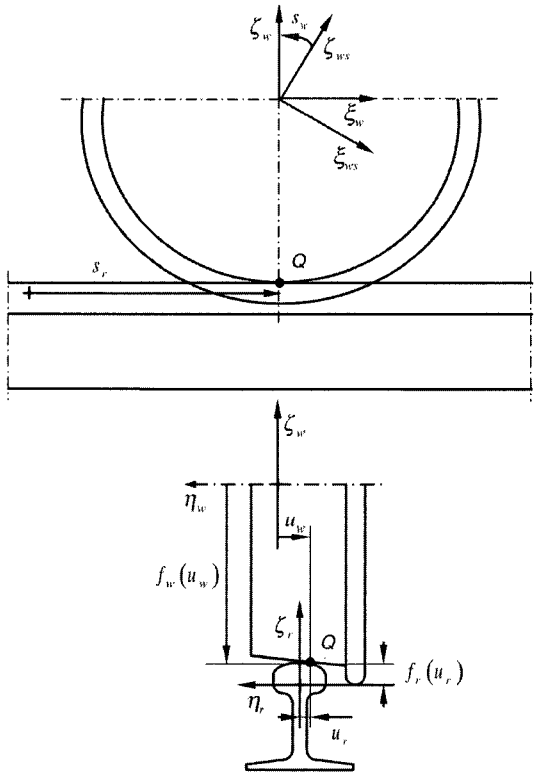

Fig. 2 Wheel and rail surface parameters

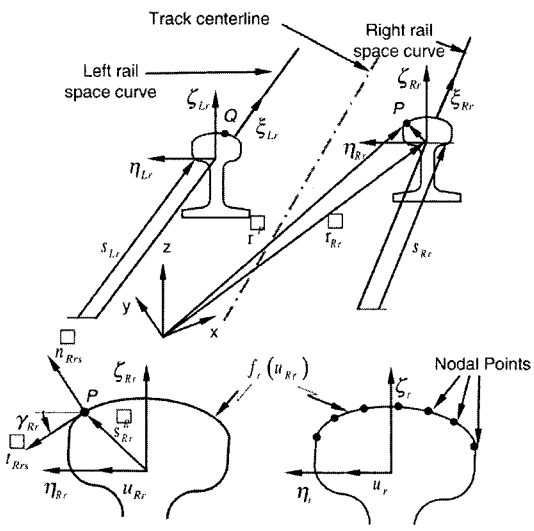

Fig. 3 Parametrization of the rail surface

profile coordinate system along the space curve can be defined in such a way that the contact point P lies in its (η_{Rr}, ζ_{Rr}) plane. The location of the origin and the orientation of the right rail profile coordinate system, defined respectively by the vector $\mathbf{r}_{Rr}$ and the transformation matrix $\mathbf{A}_{Rr}$, are uniquely determined using the surface parameter S_r (Berzeri, 2000). The location of the contact point P on the rail surface is

$$\mathbf{r}^P=\mathbf{r}_{Rr}+\mathbf{A}_{Rr}\mathbf{s}'^P_{Rr} \tag{2}$$

where $\mathbf{s}'^P_{Rr}$ is the position vector that defines the location of the contact point P on the profile coordinate system. The transformation matrix $\mathbf{A}_{Rr}$ is a function of the unit vectors that define the moving reference frame associated to the right rail space curve. In railway applications, the function f_r that defines the rail profile is a function of the surface parameter u_r using a piecewise cubic interpolation scheme (De Boor, 1978). Hence, to obtain $f_r(u_r)$, the user only has to define a set of control points that are representative of the rail profile geometry, as shown in Figure 3.

The detection of the location of the contact points between two parametric surfaces requires the definition of the normal vector to the rail surface $\mathbf{n}_{rs}$ at the point of contact

$$\mathbf{n}_{Rrs}=\mathbf{A}_{Rr}\mathbf{n}'_{Rrs} \tag{3}$$

where $n'_{Rrs}=\{0,\ \cos\gamma_{Rrs},\ \sin\gamma_{Rrs}\}^T$ is the unit vector normal to the rail surface, defined in the profile coordinate system. This vector is obtained through the contact angle γ_{Rrs}, shown in Figure 3. The contact angle is

$$\gamma_{Rrs}=\mathrm{tg}^{-1}\left(\frac{df_r(u_{Rr})}{du_{Rr}}\right) \tag{4}$$

The surface of revolution of each wheel is generated by a complete rotation, about the wheel axis, of the two-dimensional curve that defines the wheel profile (Shabana, 2001). Figure 4 shows the left wheel with arbitrary surface profile assembled in a wheelset. The surface geometry of the wheel is described using the two surface parameters S_w and u_w that represent the

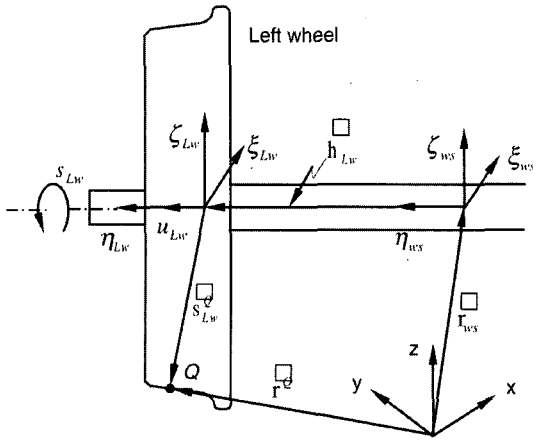

Fig. 4 Parametrization of the wheel surface

rotation of the wheel profile coordinate system (ξ_w, η_w, ζ_w) with respect to the wheelset coordinate system $(\xi_{ws}, \eta_{ws}, \zeta_{ws})$, and the lateral position of the contact point in the wheel profile coordinate system. The location of the origin and the orientation of the wheelset frame are defined by vector $\mathbf{r}_{ws}$ and matrix $\mathbf{A}_{ws}$. The global position of an arbitrary point on the wheel is

$$\mathbf{r}^Q_{Lw}\mathbf{r}_{ws}+\mathbf{A}_{ws}(\mathbf{h}_{Lw}+\mathbf{A}_{Lw}\mathbf{s}'^Q_{Lw}) \tag{5}$$

where $\mathbf{h}_{Lw}=\{0\ \ 1/2H\ \ 0\}^T$ is the local position vector that defines the location of the profile coordinate system with respect to the wheelset reference frame, being H the lateral distance to the wheel profile origin. $\mathbf{s}'^Q_{Lw}$ and $\mathbf{s}'^P_{Rw}$ are the local position vectors that define the location of the contact points Q on the wheel surfaces with respect to the profiles coordinate systems, i.e.

$$\mathbf{s}'^Q_{Lw}=\{0\ \ u_{Lw}\ \ f_w(u_{Lw})\}^T \tag{6}$$

To use the multibody contact model to solve the problem of wheel-rail contact it is necessary to devise a strategy to determine the location of the contact points between two parametric surfaces. This formulation requires that the parametric surfaces are convex. Therefore, the wheel profile is represented by two independent functions f^t_w and f^f_w that parameterize the wheel tread and flange, respectively. The search for the location of the contact points requires the definition of two tangent vectors to the wheel surface, t_{w1} and t_{w2},

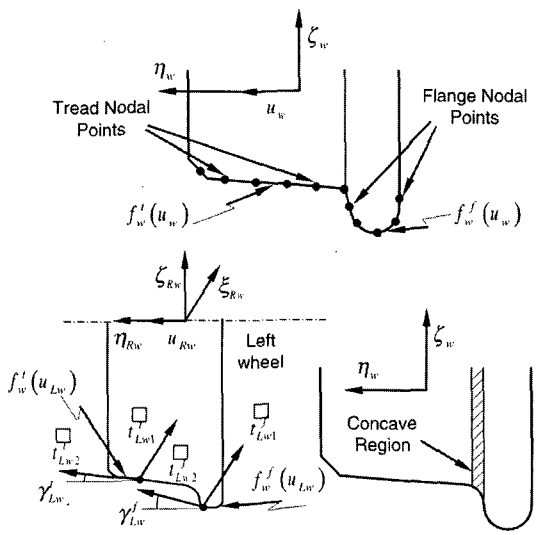

Fig. 5 Wheel profile and parametrization

at the point of contact

$$\begin{aligned}\mathbf{t}^l_{Lw1}&=\mathbf{A}_{ws}\,\mathbf{A}_{Lw}\,\mathbf{t}'^l_{Lw1};\ l=t,\ f\\ \mathbf{t}^l_{Lw2}&=\mathbf{A}_{ws}\,\mathbf{A}_{Lw}\,\mathbf{t}'^l_{Lw2};\ l=t,\ f\end{aligned}\tag{7}$$

where $\mathbf{t}'^l_{Lw1}=\{1\ 0\ 0\}^T$ and $\mathbf{t}'^l_{Lw2}=\{0\ \cos\gamma^l_{Lw}\ \sin\gamma^l_{Lw}\}^T$. The quantities with superscripts $(.)^t$ and $(.)^f$ are referred to the wheel tread and flange respectively. The contact angle is

$$\gamma^l_{Lw}=\mathrm{tg}^{-1}\left(\frac{df^l_w(u^l_{Lw})}{du^l_{Lw}}\right);\ l=t,\ f\tag{8}$$

4. Wheel-rail contact model

The location of the contact points between the wheel and the rail is complicated since both are profiled. Furthermore, the large amount of parameters that include the shape of the surfaces in contact, relative contact velocities, contact forces, and physical properties of the materials, unavoidably lead to complex theories to find the contact forces.

4.1 Wheel-rail contact detection

Consider two generic surfaces i and j depicted in Figure 6 defined by the parametric functions $\mathbf{p}(u,\ w)$, and $\mathbf{q}(s,\ t)$, respectively. The minimum distance between the two patches $\mathbf{p}(u,\ w)$

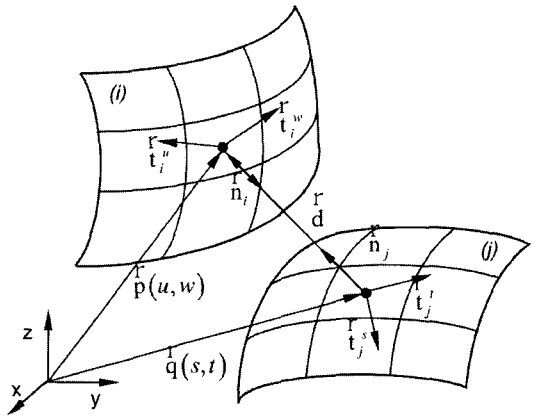

Fig. 6 Contact points on two surfaces

and $\mathbf{q}(s,\ t)$ is given by

$$\mathbf{d}=\mathbf{p}(u,\ w)-\mathbf{q}(s,\ t)\tag{9}$$

The tangent vectors $\mathbf{t}^u_i$, $\mathbf{t}^w_i$, $\mathbf{t}^s_j$ and $\mathbf{t}^t_j$ to the parametric surfaces, shown in Figure 6, are defined as:

$$\begin{aligned}\mathbf{t}^u_i&=\frac{\partial\mathbf{p}(u,\ w)}{\partial u};\ \mathbf{t}^w_i=\frac{\partial\mathbf{p}(u,\ w)}{\partial w};\\ \mathbf{t}^u_i&=\frac{\partial\mathbf{q}(s,\ t)}{\partial s};\ \mathbf{t}^t_i=\frac{\partial\mathbf{q}(s,\ t)}{\partial t}\end{aligned}\tag{10}$$

The normal unit vectors to the parametric surfaces, are

$$\mathbf{n}_i=\frac{\tilde{\mathbf{t}}^u_i\,\mathbf{t}^w_i}{\|\tilde{\mathbf{t}}^u_i\,\mathbf{t}^w_i\|};\ \mathbf{n}_j=\frac{\tilde{\mathbf{t}}^s_j\,\mathbf{t}^t_j}{\|\tilde{\mathbf{t}}^s_j\,\mathbf{t}^t_i\|}\tag{11}$$

For the wheel-rail contact problem the equations that define the candidates to contact points, represented in situations Figure 7(a), (b) and (c) II, are

(i) The surfaces normals $\mathbf{n}_i$ and $\mathbf{n}_j$ at the candidates to contact points have to be parallel:

$$\mathbf{n}_j\times\mathbf{n}_i=0\Longleftrightarrow\begin{cases}\mathbf{n}^T_j\,\mathbf{t}^u_i=0\\ \mathbf{n}^T_j\,\mathbf{t}^w_i=0\end{cases}\tag{12}$$

(ii) The vector $\mathbf{d}$ has to be parallel to the normal vector $\mathbf{n}_i$:

$$\mathbf{d}\times\mathbf{n}_i=0\Longleftrightarrow\begin{cases}\mathbf{d}^T\,\mathbf{t}^u_i=0\\ \mathbf{d}^T\,\mathbf{t}^w_i=0\end{cases}\tag{13}$$

(iii) The contact condition specifies that:

$$\mathbf{d}^T\,\mathbf{n}_j\le 0\tag{14}$$

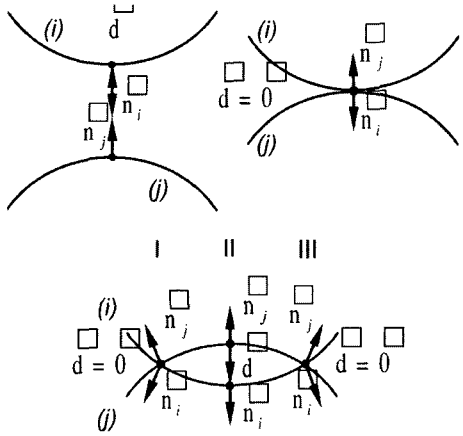

Fig. 7 (a) No contact; (b) Contact at a single point; (c) Contact with penetration

The geometric conditions in equations (12) and (13) are four nonlinear equations with four unknowns, which are the surfaces parameters u, w, s and t. In the computational implementation, the information of a previous time step is used as initial estimate for the solution search of the equations.

4.2 The two point contact scenario

More than one pair of contact points can develop between the wheel and the rail wheel, as shown in Figure 8. Let two different functions f_w^t and f_w^f parameterize, the wheel tread and flange, respectively, as shown in Figure 5. The formulation used to look for the candidates to contact points is fully independent for the wheel tread and for the wheel flange surfaces.

This methodology allows finding multiple wheel-rail contact points locations and to study the lead and lag contact configurations. Since the methodology used to look for candidates to contact points is fully independent for the wheel tread and for the wheel flange, the contact point in the flange does not have to be located in the same plane as the contact point in the wheel tread, as shown in Figure 8. This allows the analysis of derailment or of the effect of switches.

4.3 Normal contact forces in the wheel-rail

The normal contact forces are calculated using the contact force model proposed by Lankarani and Nikravesh (1995), which requires the amount of penetration, the relative velocity between the contact point and the material properties of the wheel and rail. The direction of the normal forces is determined from the wheel and rail profile data. The evaluation of the normal contact force is

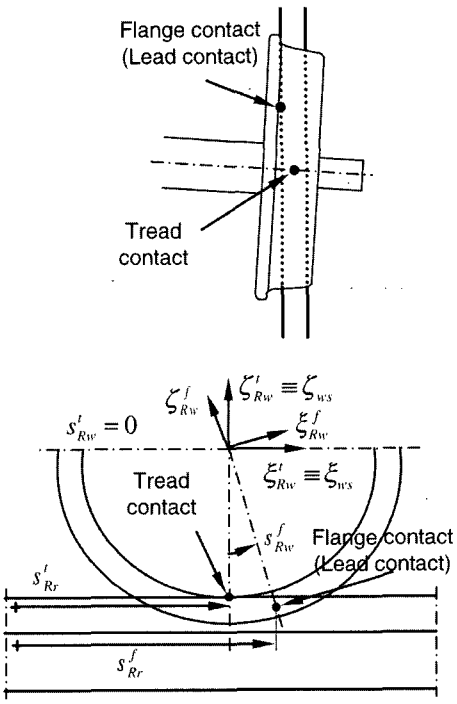

Fig. 8 Lead and lag contact in wheel-rail

$$N = K\left(1 + \frac{3(1-e^2)}{4}\frac{\dot{\delta}}{\dot{\delta}^{(-)}}\right)\delta^n \qquad (15)$$

where δ is the indentation, $n=1.5$ is the parameter used for metal to metal contact, K is the Hertzian constant that depends on the surface curvatures and the elastic properties of contacting bodies, $\dot{\delta}$ is the coefficient of restitution, $\dot{\delta}^{(-)}$ is the velocity of indentation and is the velocity of indentation at the initial instant of contact, both evaluated as the projection of the relative velocity vector of the point of contact on the vector normal to the contact surfaces.

4.4 Tangential contact forces

Knowing the normal contact forces that develop between the wheel and rail and the creepages, i.e., the relative velocities, it is possible to calcu-

late the tangential contact forces using one of the models available in the literature. Three models are presented here in order to allow for a comparative study between them to be developed.

The Kalker Linear evaluates the longitudinal F_ξ and lateral F_η components of the creep force and the spin creep moment M_ϕ, that develop in the wheel-rail contact region as

$$\begin{Bmatrix} F_\xi \\ F_\eta \\ M_\phi \end{Bmatrix} = Gab \begin{bmatrix} c_{11} & 0 & 0 \\ 0 & c_{22} & \sqrt{ab}\, c_{23} \\ 0 & -\sqrt{ab}\, c_{23} & ab\, c_{33} \end{bmatrix} \begin{Bmatrix} v_\xi \\ v_\eta \\ \phi \end{Bmatrix} \quad (16)$$

where G is the combined shear modulus of rigidity of wheel and rail materials and a and b are the semi-axes of the contact ellipse. The parameters c_{ij} are the Kalker creepage and spin coefficients, obtained in references (Kalker, 1990; Garg, 1984). The quantities v_ξ, v_η and ϕ represent the longitudinal, lateral and spin creepages at the contact point, respectively. For sufficiently small values of creep and spin, the linear theory of Kalker is adequate to determine the creep forces. For larger values, this formulation is no more appropriated since it does not include the saturation effect of the friction forces, i.e., it does not assure that $F_v \leq \mu N$.

The Heuristic Nonlinear Force Model involves calculating the creep force expected from the Kalker linear theory and modifying it by a factor that takes into account the limiting creep force (Shen, 1983). First, the resultant creep force of Kalker linear theory is calculated

$$F_v' = \sqrt{F_\xi'^2 + F_\eta'^2} \quad (17)$$

where the notation $(.)'$ now means that the quantities are obtained with the Kalker's linear theory. The limiting resultant creep force is determined by:

$$F_v = \mu N \begin{cases} \left[\left(\frac{F_v'}{\mu N}\right) - \frac{1}{3}\left(\frac{F_v'}{\mu N}\right)^2 + \frac{1}{27}\left(\frac{F_v'}{\mu N}\right)^3\right] & \text{if } F_v' \leq 3\mu N \\ 1 & \text{if } F_v' > 3\mu N \end{cases} \quad (18)$$

where μ is the friction coefficient. The new resultant creep force F_v is used to calculate the tangential forces as:

$$F_\xi = \frac{F_v}{F_v'} F_\xi' \; ; \; F_\eta = \frac{F_v}{F_v'} F_n' \quad (19)$$

In the Heuristic method the spin creep moment M_ϕ is neglected. This theory gives more realistic values for creep forces outside the linear range than the Kalker's linear theory. For high values of spin, the Heuristic theory can lead to unsatisfactory results (Andersson, 1998).

In the Polach Nonlinear Force Model the longitudinal and lateral components of the creep force are (Polach, 1999)

$$F_\xi = F\frac{v_\xi}{v_c} \; ; \; F_\eta = F\frac{v_\eta}{v_c} + F_{\eta s}\frac{\phi}{v_c} \quad (20)$$

where F is the tangential contact force caused by longitudinal and lateral creepages, v_c is the modified translational creepage, which accounts the effect of spin creepage, and $F_{\eta s}$ is the lateral tangential force caused by spin creepage. The Polach algorithm takes, as input, the creepages v_ξ, v_η and ϕ, the normal contact force N, the semi-axes a and b of the contact ellipse, the combined modulus of rigidity of wheel and rail materials G, the friction coefficient μ and the Kalker creepage and spin coefficients c_{ij}. The Polach algorithm is suitable to study the tangential contact forces that develop in the wheel-rail interface. This method allows the calculation of full nonlinear creep forces and takes spin into account.

5. Application to a Railway Vehicle

The ML95 trainset, shown in Figure 9, is used by the Lisbon metro company (ML). The ML95

Fig. 9 The ML95 trainset

trainset is an electrical three-car unit composed of two powered end vehicles with driving cabs, and a intermediate vehicle, represented in Figure 10.

Each ML95 trailer vehicle is composed of one carbody where the passengers travel, supported by two bogies through the secondary suspension, which is set to minimize the vibrations induced by the track on the passenger compartment. The bogies are the subsystems that, through the wheelsets, are in contact with the track and include the primary suspension, which is the main responsible for the steering capabilities and stability behavior.

Each trailer bogie of the ML95 consists of one frame, two wheelsets, four axleboxes and the mechanical elements that compose the primary suspension. The bogie frame is supported by the axleboxes through eight metal-rubber springs of the "Chevron" type. The vertical displacements of the primary suspension are limited by bumpstops and liftstops, shown in Figure 11.

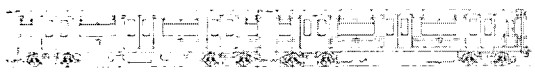

Fig. 10 Schematic representation of the ML95

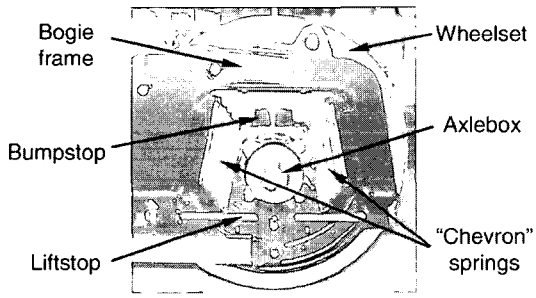

Fig. 11 Primary suspension of the trailer bogie

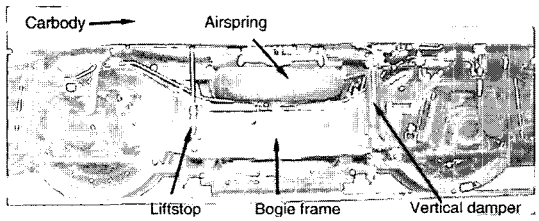

Fig. 12 Secondary suspension of the trailer bogie

The trailer vehicle carbody is supported by four airsprings, and with each one there is a vertical "Chevron" bumpstop assembled in series. In parallel with the airsprings, four vertical hydraulic dampers and four vertical liftstops devices, shown in Figure 12, are mounted. The connection between the carbody and each bogie is done by a shaft, which guarantees an appropriate and stable rotation of the bogie with respect to the carbody. The mechanical elements that assure the connection between each bogie and the carbody are mounted between a center plate and the bogie frame, as shown in Figure 13.

The transmission of traction and braking efforts between each bogie and the carbody is done by traction rods. The lateral stabilization of the carbody needs two transversal hydraulic dampers, between the center plate and bogie frame. The characteristics of the ML95 trainset are shown in Table 1.

The model of the railway vehicle leads to representation of the multibody model shown in Figure 14. The mass and inertia properties of system components have been supplied by the manufacturer company. For bodies with no data

Table 1 Main characteristics of the ML95 vehicle

Traffic velocity range	40−60 Km/h
Minimum curve radius on track	60 m
Track gauge	1.435 m
Wheel rolling radius new	0.43 m
Bogie wheelbase	2.1 m
Bogie center distance	11.1 m
Wheelset weight	1109 Kg
Bogie weight	4200 Kg
Weight of the carbody	11160 Kg
Floor height	1.155 m
Vehicle height	3.523 m
Vehicle width	2.789 m
Vehicle length	15.30 m

Fig. 13 Bogie-carbody connection of the vehicle

available, the mass and inertia properties are estimated based on their geometry. The location and type of kinematic joints is also obtained with the manufacturers information.

The first simulation scenario used to apply the methodology developed corresponds to a straight track with no irregularities in which a vehicle with new wheels runs. The starting position of the vehicle is such that the model is misaligned by 2 mm relative from the track centerline. The results of the simulation, for several velocities, are represented by the lateral displacements of the wheelsets presented in Figure 15. In all cases the Polach formulation has been used to calculate the creep forces.

It is observed that for vehicle forward velocities under 60 m/s the wheelset undergoes lateral decaying oscillations and returns to the center of the track. This indicates a stable running of the vehicle. At sufficiently high speeds, 70 m/s for instance, the lateral oscillations increase and the vehicle derails. By running the vehicle at intermediate speeds it is observed that the critical speed of the vehicle is 60.5 m/s.

To appraise the difference between the different force models, several vehicle simulations are done for a velocity of 50 m/s. The results for the vertical and lateral wheel forces are represented in Figures 16 and 17, respectively. It is observed that for all creep models the results obtained are similar. This is expected results since there are no high creepages at the speeds considered.

To evaluate the performance of different creep models the vehicle is simulated, for velocities of 10 and 20 m/s, in a scenario where the track has a curved geometry, as shown in Figure 18. The dashed lines represent transition segments with 50 m. For both simulation velocities the contact forces obtained with Kalker linear theory lead to the lift of the outer wheel of the front wheelset, as shown in Figure 19. Derailment does not occur

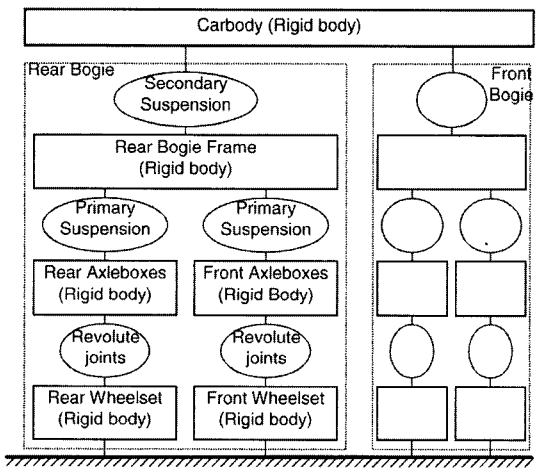

Fig. 14 Vehicle multibody model

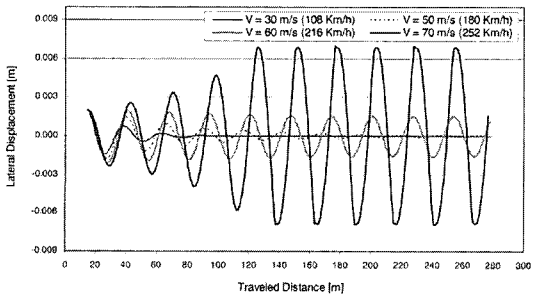

Fig. 15 Lateral displacement of the front wheelset

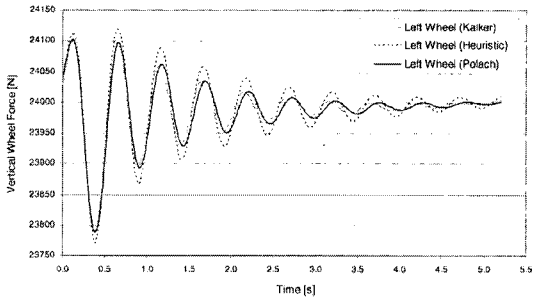

Fig. 16 Vertical forces on one wheel for a velocity of 50 m/s for the three creep models

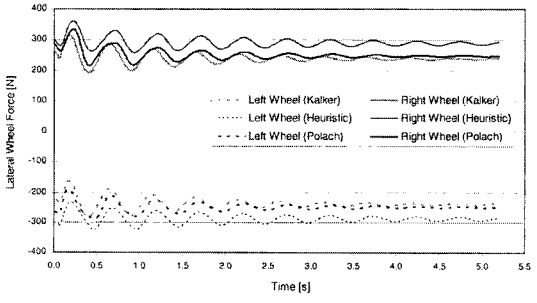

Fig. 17 Lateral forces on one wheel for a velocity of 50 m/s for the three creep models

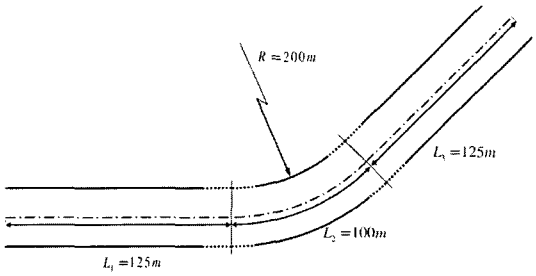

Fig. 18 Curved track geometry

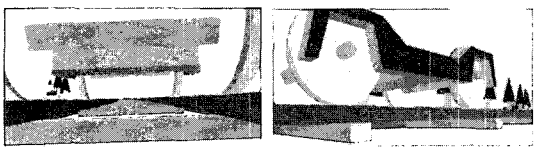

Fig. 19 Lifting of the right front wheel when using the Kalker linear theory

due to the flange contact. Since high creepages are involved the Kalker linear theory is inappropriate to compute the creep forces. It is suggested that for cases that involve curved tracks or running speeds closer to the critical speeds the Heuristic or the Polach creep force models should be selected. Based on results not shown in this paper, due to space restrictions, it can be shown that the Polach nonlinear force model is superior, and more efficient from the computational point of view, than the other two force models considered.

Another aspect worth checking concerns the different parametrization schemes for the rail curves. All results of the contact force models are dependent on their geometric correctness. Two cubic parameterization schemes are tested: Cubic Splines, which is probably the most popular interpolation scheme used; Shape Preserving Splines, which maintain the curvature of the segments faithful to that of the original data. Several simulations of the vehicle are carried for the curved track parameterized with the two types of splines. In all simulations only the Polach force model is used. Selected results for the vertical and lateral forces in the wheel are presented in Figures 20 and 21.

In Figure 20 it can be observed that the Cubic splines lead to a response that contains very pronounced peaks for times close to 14 and 19

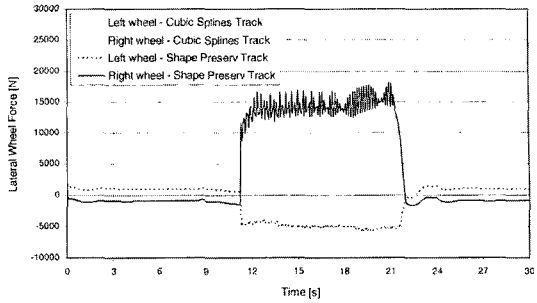

Fig. 20 Lateral contact forces on the leading wheelset for a forward velocity of 10 m/s

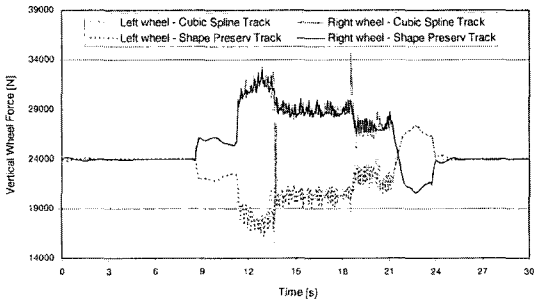

Fig. 21 Vertical contact forces on the leading wheelset for a forward velocity of 10 m/s

sec. These type of peaks are always present in interpolations involving cubic splines and lead to a perception of the system response associated with high perturbations. However, these perturbations have no physical content and, therefore, the interpolation of curved tracks based on cubic splines can be misleading. These type of peaks are not present when the track is obtained with the shape preserving splines interpolation. Note also that the vertical wheel forces obtained for tracks interpolated by these two schemes exhibits the same isolated high peaks that lead to the same conclusions. These problems are not observed with tangent tracks because all interpolating splines lead to similar curves.

6. Conclusion

A new methodology was proposed to identify the contact points between the wheel and the rail. This procedure allows that two simultaneous contact points to be identified, allowing to study track switches and problems involving derail-

ment. The application of the procedures to the simulation of a railway vehicle in different scenarios made it possible to identify its critical velocity and to evaluate the virtues and drawbacks of different track interpolation schemes and creep force models. The results show that the use of cubic splines for the rails and wheels leads to spurious oscillations on the contact forces. It is concluded that shape preserving splines is the most advantageous cubic polynomial interpolation process. Among the three creep force models tested it was shown that the Polach nonlinear force model is the only one that is suitable for all simulations carried. The Kalker linear force model fails when the tangential forces reach their saturation level. The Heuristic model leads to less accurate results for flange contact, when there are high creepages involved.

Acknowledgment

The support of Fundação para a Ciencia e Técnologia (FCT) through the grant BD/18180/98, is gratefully acknowledged.

References

Andersson, E., Berg, M. and Stichel, S., 1998, *Rail Vehicle Dynamics, Fundamentals and Guidelines*, Royal Institute of Technology (KTH), Stockholm, Sweden.

Berzeri, M., Sany, J. and Shabana, A., 2000, Curved Track Modeling Using the Absolute Nodal Coordinate Formulation, Technical Report MBS00-4-UIC, Department of Mechanical Engineering, University of Illinois, Chicago.

De Boor, C. A., 1978, *Practical Guide to Splines*, Springer-Verlag, New York, New York.

Garg, V. and Dukkipati, R., 1984, *Dynamics of Railway Vehicle Systems*, Academic Press, New York, New York.

Kalker, J., 1996, *Book of Tables for the Hertzian Creep-Force Law*, Report of the Faculty of Technical Mathematics and Informatics No. 96-61, Delft University of Technology, Delft, The Netherlands.

Kalker, J., 1979, "The Computation of Three-Dimensional Rolling Contact with Dry Friction," *Numerical Methods in Engineering*, 14(9), pp. 1293~1307.

Kalker, J., 1990, *Three-Dimensional Elastic Bodies in Rolling Contact*, Kluwer Academic Publishers, Dordrecht, The Netherlands.

Kik, W. and Piotrowski, Fast, J. A., 1996, "Approximate Method to Calculate Normal Load at Contact Between Wheel and Rail and Creep Forces During Rolling," *2nd Mini Conference on Contact Mechanics and Wear of Rail/Wheel System*, TU Budapest, Budapest, Hungary.

Lankarani, H. M. and Nikravesh, P. E., 1994, "Continuous Contact Force Models for Impact Analysis in Multibody Systems," *Nonlinear Dynamics*, 5, pp. 193~207.

Polach, O., 1999, "A fast Wheel-Rail Forces Calculation Computer Code," *Vehicle System Dynamics*, Sup 33, pp. 728~739.

Pombo, J. and Ambrosio, J., 2003, "A General Track Model for Rail Guided Vehicles Dynamics," *VII Congresso de Mecanica Aplicada e Computacional*, April 14-16, Evora, Portugal, pp. 47~56a.

Pombo, J. and Ambrosio, J., 2003b, "A Wheel-Rail Contact Model for Rail Guided Vehicles Dynamics," *ECCOMAS Conference Multibody 2003 - Advances in Computational Multibody Dynamics*, July 1-4, Lisbon, Portugal.

Pombo, J. and Ambrosio, J., 2001, "General Spatial Curve Joint for Rail Guided Vehicles: Kinematics and Dynamics," *Multibody Systems Dynamics*, 9, No. 237~264.

Shabana, A., Berzeri, M. and Sany, J., 2003c, "Numerical Procedure for the Simulation of Wheel/Rail Contact Dynamics," *Journal of Dynamic Systems Measurement and Control-Transactions of the Asme*, 123(2), pp. 168~178.

Shen, Z., Hedrick, J. and Elkins, J., 1983, "Comparison of Alternative Creep Force Models for Rail Vehicle Dynamic Analysis," *Proc. of 8th IAVSD Symp on Dynamics of Vehicles on Road and Tracks*, Cambridge, Massachussetts pp. 591~605.